Conference Proceedings of the Society for Experimental Mechanics Series

Chad Walber
Matthew Stefanski
Steve Seidlitz *Editors*

Sensors and Instrumentation, Aircraft/Aerospace, Energy Harvesting & Dynamic Environments Testing, Volume 7

Proceedings of the 39th IMAC, A Conference and Exposition on Structural Dynamics 2021

Springer

Conference Proceedings of the Society for Experimental Mechanics Series

Series Editor

Kristin B. Zimmerman, Ph.D.
Society for Experimental Mechanics, Inc.,
Bethel, CT, USA

The Conference Proceedings of the Society for Experimental Mechanics Series presents early findings and case studies from a wide range of fundamental and applied work across the broad range of fields that comprise Experimental Mechanics. Series volumes follow the principle tracks or focus topics featured in each of the Society's two annual conferences: IMAC, A Conference and Exposition on Structural Dynamics, and the Society's Annual Conference & Exposition and will address critical areas of interest to researchers and design engineers working in all areas of Structural Dynamics, Solid Mechanics and Materials Research

More information about this series at http://www.springer.com/series/8922

Chad Walber • Matthew Stefanski • Steve Seidlitz
Editors

Sensors and Instrumentation, Aircraft/Aerospace, Energy Harvesting & Dynamic Environments Testing, Volume 7

Proceedings of the 39th IMAC, A Conference and Exposition on Structural Dynamics 2021

Springer

Editors
Chad Walber
PCB Piezotronics, Inc
Depew, NY, USA

Steve Seidlitz
Minneapolis, MN, USA

Matthew Stefanski
Dayton, OH, USA

ISSN 2191-5644 ISSN 2191-5652 (electronic)
Conference Proceedings of the Society for Experimental Mechanics Series
ISBN 978-3-030-75987-2 ISBN 978-3-030-75988-9 (eBook)
https://doi.org/10.1007/978-3-030-75988-9

This Springer imprint is published by the registered company Springer Nature Switzerland AG
The registered company address is: Gewerbestrasse 11, 6330 Cham, Switzerland

Preface

Sensors and Instrumentation, Aircraft/Aerospace, Energy Harvesting & Dynamic Environments Testing represents one of nine volumes of technical papers presented at the 39th IMAC, A Conference and Exposition on Structural Dynamics, organized by the Society for Experimental Mechanics, and held between February 8 and 11, 2021. The full proceedings also include volumes on nonlinear structures and systems; dynamic substructures; model validation and uncertainty quantification; dynamic substructures; special topics in structural dynamics and experimental techniques; rotating machinery, optical methods, and scanning LDV methods; topics in modal analysis and parameter identification; and data science in engineering.

Each collection presents early findings from experimental and computational investigations on an important area within sensors and instrumentation and other structural dynamics areas. Topics represent papers on calibration, smart sensors, practical issues improving energy harvesting measurements, shock calibration and shock environment synthesis, and applications for aircraft/aerospace structures.

The organizers would like to thank the authors, presenters, session organizers, and session chairs for their participation in this track.

Depew, NY, USA — Chad Walber

Dayton, OH, USA — Matthew Stefanski

Minneapolis, MN, USA — Steve Seidlitz

Contents

Chapter 1
Exploring Iterative Optimization Methods to Develop a MIMO Control Input

J. Justin Wilbanks, Ryan A. Schultz, and Brian C. Owens

Abstract In general, existing methods to develop an effective input for multiple-input/multiple-output (MIMO) control do not offer flexibility to account for limitations in experimental test setups or tailor the control to specific test objectives. The work presented in this paper introduces a method to leverage global optimization approaches to define a MIMO control input to match a data set representing field data. This contrasts with traditional MIMO input estimation methods which rely on direct inverse methods. Efficacy of the iterative optimization method depends on the objective function and optimization method used as well as the definition of the format of the input cross-power spectral density (CPSD) matrix for the optimization routine. Various objective functions are explored in this work through sampling as well as implementation within the iterative optimization process and their impact on the resulting output CPSD. Performance of iterative optimization is assessed against the traditional, direct pseudoinverse method of obtaining the input CPSD as well as the buzz method and weighted least squares (LS). Constraints can be used within the optimization process to control the magnitude and other aspects of the input CPSD, which allows for shaker limitations to be accounted for, among other considerations. Iterative optimization can provide the best input CPSD possible for a test setup while accounting for any shortcomings the setup may have, including force and voltage constraints, which is not possible with traditional methods.

Keywords MIMO control · Global optimization methods · Vibration testing · Dynamic modeling · Multi-axis testing

1.1 Introduction

Multiple-input/multiple-output (MIMO) control methodologies are becoming more common in the structural dynamics community alongside multi-axis vibration testing due to the benefits that multi-axis tests have compared to traditional single-axis vibration testing [1]. Free-free MIMO vibration testing provides effective reproduction of the aerodynamic operating environments of vehicles unlike single-axis testing that creates representations that often differ significantly from the operating environments [1, 2]. Daborn et al. showed single-axis testing can alter the dynamics of the test article due to attachment to a shaker and can lead to poor recreation of stress and strain patterns in the test article arising from relative phase deviations in response locations that causes unrealistic failure modes [1]. Various papers have shown the successful recreation of aerodynamic environments for flight vehicles with multi-axis testing [3–5]. Traditional methods in acquiring the input cross-power spectral density (CPSD) to recreate a set of field data do not offer substantial flexibility in terms of constraining the voltage or force required at the shakers used in the test. Using iterative optimization allows for various constraints to be applied to the developed input while limiting the impact on the dB error or other objective function. The following sections of the paper introduce the MIMO control problem for iterative optimization, which is used to observe the impact of the optimization process, objective function, and input constraints on the efficacy of the input derived through optimization relative to traditional methods.

Sandia National Laboratories is a multimission laboratory managed and operated by the National Technology and Engineering Solutions of Sandia, LLC., a wholly owned subsidiary of Honeywell International, Inc., for the US Department of Energy's National Nuclear Security Administration under contract DE-NA0003525.

J. J. Wilbanks (✉) · R. A. Schultz · B. C. Owens
Sandia National Laboratories, Albuquerque, NM, USA
e-mail: jjwilba@sandia.gov

C. Walber et al. (eds.), *Sensors and Instrumentation, Aircraft/Aerospace, Energy Harvesting & Dynamic Environments Testing, Volume 7*, Conference Proceedings of the Society for Experimental Mechanics Series, https://doi.org/10.1007/978-3-030-75988-9_1

1.2 Definition of MIMO Control Problem for Iterative Optimization

1.2.1 Design Variable Choice to Account for Input and Output CPSD Constraints

To set up the MIMO control problem for iterative optimization, a set of design variables must be chosen to ensure that the resulting input CPSD, S_{xx}, is positive definite. The forward MIMO control problem can be defined as:

$$S_{\mathrm{yy}} = H_{\mathrm{yx}} S_{\mathrm{xx}} {H_{\mathrm{yx}}}^{\mathrm{H}} \tag{1.1}$$

where S_{xx} denotes the input CPSD that must be positive definite, S_{yy} the output CPSD, H_{yx} the transfer function matrix, and $(\,)^H$ the conjugate transpose. To ensure S_{xx} is positive definite, the design variables for the iterative optimization process are entries in an upper triangular matrix, L_{mat}, that is used to create the input CPSD matrix using a Cholesky factorization:

$$S_{xx} = L_{\mathrm{mat}}^{H} L_{\mathrm{mat}} \tag{1.2}$$

where L_{mat} is stored using a vector form within the optimization process:

$$[L_{\mathrm{mat}}] = \begin{bmatrix} L_{1,1} & L_{1,2} & \dots & L_{1,n} \\ 0 & L_{2,2} & \dots & L_{2,n} \\ \vdots & \vdots & \ddots & \vdots \\ 0 & 0 & 0 & L_{n,n} \end{bmatrix} \rightarrow \{L_{vec}\} = \begin{Bmatrix} L_{1,1} \\ L_{1,2} \\ L_{2,2} \\ \vdots \\ L_{1,n} \\ L_{2,n} \\ \vdots \\ L_{n,n} \end{Bmatrix} \tag{1.3}$$

where $L_{i,\,p}$ denotes the element of the L_{mat} matrix in the i^{th} row and p^{th} column and n the number of input locations for the MIMO control problem. Optimization with design variables chosen to be entries in the L_{mat} matrix enforces positive definiteness S_{xx}, which is not the case if optimization is performed with auto-power spectral densities (APSDs) and cross-terms of S_{xx} as design variables or APSDs, coherence, and phase. The design variable choice can be used alongside various optimization algorithms and objective functions.

1.2.2 Optimization Workflow

Optimization is performed at discrete frequency lines for a set of field data using the elements of $L_{\mathrm{vec,\,dv}}$ as the design variables, where $L_{\mathrm{vec,\,dv}}$ is defined as:

$$\left\{L_{\mathrm{vec,dv}}\right\} = \begin{Bmatrix} \left\{L_{\mathrm{vec,Re}}\right\} \\ \left\{L_{\mathrm{vec,Im}}\right\} \end{Bmatrix} \tag{1.4}$$

where $L_{\mathrm{vec,\,Re}}$ and $L_{\mathrm{vec,\,Im}}$ contain the elements of the triangular matrices $L_{\mathrm{mat,\,Re}}$and $L_{\mathrm{mat,\,Im}}$ used to form the real and imaginary portions of S_{xx} with the Cholesky factorization introduced in Eq. (1.2), respectively. The Cholesky factorization of the real and imaginary portions of S_{xx} is:

$$\begin{aligned} S_{\mathrm{xx,Re}} &= {L_{\mathrm{mat,Re}}}^{H} L_{\mathrm{mat,Re}} \\ S_{\mathrm{xx,Im}} &= {L_{\mathrm{mat,Im}}}^{H} L_{\mathrm{mat,Im}} \\ S_{\mathrm{xx}} &= S_{\mathrm{xx,Re}} + j * S_{\mathrm{xx,Im}} \end{aligned} \tag{1.5}$$

where $S_{\mathrm{xx,\,Re}}$ denotes the real portion of S_{xx}, $S_{\mathrm{xx,\,Im}}$ the imaginary portion of S_{xx}, $L_{\mathrm{mat,\,Re}}$ the upper triangular matrix for the Cholesky factorization of $S_{\mathrm{xx,\,Re}}$, and $L_{\mathrm{mat,\,Im}}$ the upper triangular matrix for the Cholesky factorization of $S_{\mathrm{xx,\,Im}}$. $L_{\mathrm{mat,\,Re}}$ is formed directly from $L_{\mathrm{vec,\,Re}}$. $L_{\mathrm{mat,\,Im}}$ is found using the following expressions to maintain the positive definiteness of $S_{\mathrm{xx,\,Im}}$:

$$\left[L_{\mathrm{mat,Im}}\right] = \begin{bmatrix} 0 & L_{\mathrm{mat,Im}_{1,2}} & L_{\mathrm{mat,Im}_{1,3}} & \cdots & L_{\mathrm{mat,Im}_{1,2}} \\ 0 & 0 & L_{\mathrm{mat,Im}_{2,3}} & \cdots & \vdots \\ \vdots & \vdots & 0 & \ddots & L_{\mathrm{mat,Im}_{n-1,2}} \\ 0 & 0 & 0 & 0 & 0 \end{bmatrix} + \begin{bmatrix} 1 & 0 & \cdots & 0 \\ 0 & 1 & \cdots & 0 \\ \vdots & \vdots & \ddots & \vdots \\ 0 & 0 & 0 & 1 \end{bmatrix} \tag{1.6}$$

where

$$\left\{L_{\mathrm{vec,Im}}\right\} = \begin{Bmatrix} L_{\mathrm{mat,Im}_{1,2}} \\ L_{\mathrm{mat,Im}_{1,3}} \\ L_{\mathrm{mat,Im}_{2,3}} \\ \vdots \\ L_{\mathrm{mat,Im}_{1,2}} \\ \vdots \\ L_{\mathrm{mat,Im}_{n-1,2}} \end{Bmatrix} \tag{1.7}$$

and $L_{\mathrm{mat,Im}_{i,p}}$ denotes one of the upper triangular terms in the i^{th} row and p^{th} column of $L_{\mathrm{mat,\,Im}}$ taken directly from $L_{\mathrm{vec,\,Im}}$, shown in Eq. (1.7). Once $S_{\mathrm{xx,\,Im}}$ is formed using Eq. (1.5), the diagonal entries resulting from the addition of the identity matrix in the definition of $L_{\mathrm{mat,\,Im}}$ are removed.

The complete optimization process can be broken down as follows:

1	Make an initial guess for the complete L matrix in the form of $L_{\mathrm{vec,\,dv}}$
2	Extract real and imaginary parts from the current guess vector, $L_{\mathrm{vec,\,dv}}$
3	Form triangular matrices, $L_{\mathrm{mat,\,Re}}$ and $L_{\mathrm{mat,\,Im}}$, from current $L_{\mathrm{vec,\,dv}}$
4	Form $S_{\mathrm{xx,\,Re}}$ and $S_{\mathrm{xx,\,Im}}$ from $L_{\mathrm{mat,\,Re}}$ and $L_{\mathrm{mat,\,Im}}$ using Eq. (1.5)
5	Form complete input matrix S_{xx} as sum of $S_{\mathrm{xx,\,Re}}$ and $S_{\mathrm{xx,\,Im}}$
6	Solve forward MIMO control problem, defined with Eq. (1.1), to get response from this optimization iteration
7	Compute one of several scalar objective functions to compare current response to the field data

where the objective functions used in this paper are explored in Sect. 1.3. In general, the S_{xx} formed using the method outlined above will be Hermitian positive definite, but numerically it could become slightly nonpositive definite. Therefore, a small correction can be applied to ensure the resulting S_{xx} is Hermitian positive definite:

$$S_{\mathrm{xx}} = S_{\mathrm{xx}} + {S_{\mathrm{xx}}}^{\mathrm{H}} - S_{\mathrm{xx_D}}$$

$$S_{\mathrm{xx_D}} = \begin{cases} S_{\mathrm{xx}} & \text{if } i = p \\ 0 & \text{otherwise} \end{cases} \tag{1.8}$$

where S_{xx_D} denotes the matrix of just the diagonal elements of S_{xx}, i the row index of a matrix element, and p the column index of a matrix element. As an additional guarantee of positive definiteness, the eigenvalues of S_{xx} are adjusted to numerically enforce the constraint, if needed. The process outlined in Steps 1–7 above are repeated until an acceptable solution is obtained based on the parameters used with the optimization algorithms implemented with DAKOTA, an optimization software created at the Sandia National Laboratories, for each frequency step within the frequency range of interest [6].

1.2.3 Example Problem Definition

The example problem used in this paper is the payload positioned at the top of the rocket assembly, modeled as a beam, as shown in blue in Fig. 1.1. Only transverse vibration is considered with two degrees of freedom, transverse displacement and rotation, for each node of the beam model.

The payload is modeled as free-free with 25 elements in total and analyzed for the chosen frequency range from 20 to 400 Hz in 1 Hz increments. Elements are defined to be solid aluminum. Modal damping is defined at 2% of critical for the system. Input for the system is applied at two locations, 50.8 cm and 533.4 cm from the bottom of the payload that attaches to the rocket assembly, with the output measured at four locations along the payload, 127 cm, 177.8 cm, 406.4 cm, and 508 cm from the payload bottom. The field environment defined for the input is a random force power spectral density (PSD) with a level of 198.0 N^2/Hz and variance of 784.3 N^4/Hz^2 down the length of the payload. Figure 1.2 shows the field input applied to the node at 50.8 cm along the payload length. The inputs from the field environment are applied to the frequency response functions (FRFs) of the system to get the response of the field environment, $S_{yy_{Field}}$. The optimization will then determine a set of inputs to best make the payload respond as it did to the field environment forces.

1.3 Exploration of Objective Functions with Sampling

Latin hypercube sampling (LHS) is completed within the DAKOTA framework for the example problem to observe the sensitivity of the objective functions (OFs) to the elements of $L_{vec,\,dv}$ with a near random sampling [6]. There is not a well-accepted OF for the optimization problem presented in this paper. Therefore, three OFs are explored in this paper to determine the best function to use in order to acquire an output APSD sum that closely follows the field value. The OFs used are output CPSD dB error, output CPSD mean squared error, and output APSD sum error. The output CPSD dB error is calculated as:

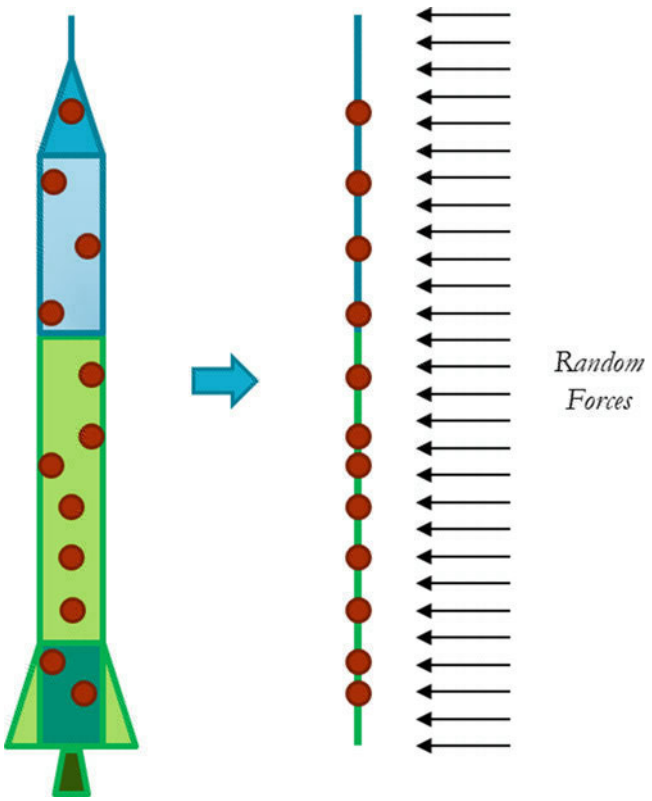

Fig. 1.1 Example beam model representing rocket with payload attached for MIMO input development with iterative optimization (Note: Nodes shown are only for example to show modeling methodology)

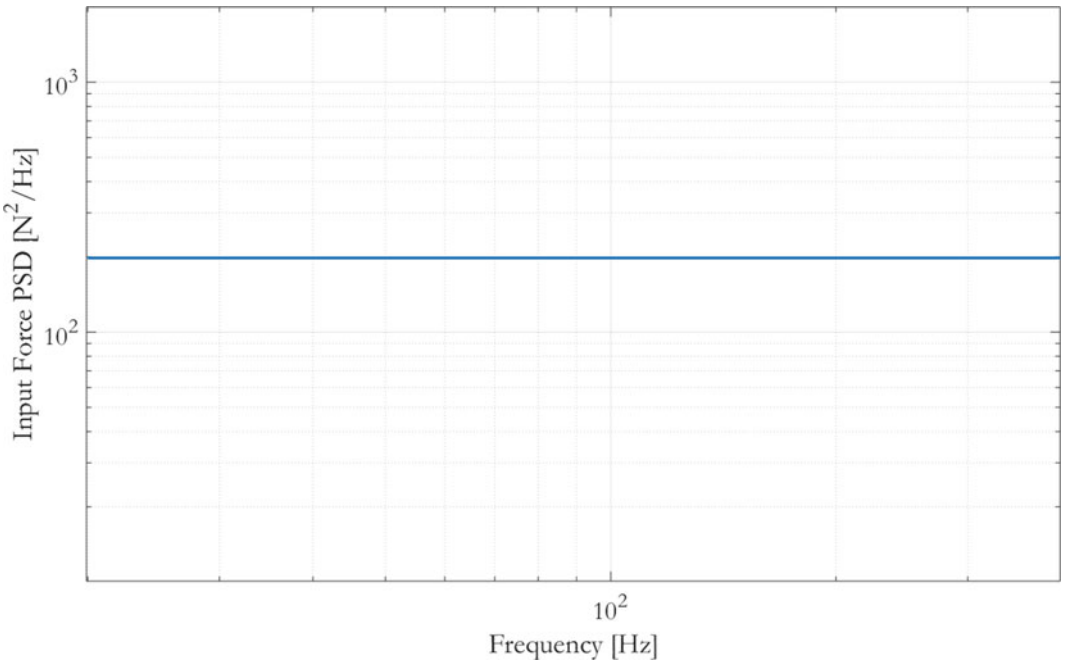

Fig. 1.2 Random force PSD applied at Input Node 1 (50.8 cm) along the payload

$$\mathrm{OF}_{\mathrm{dB}} = \left\| \mathrm{Error}_{\mathrm{dB,UT}} * W \right\|_1 \tag{1.9}$$

$$\mathrm{Error}_{\mathrm{dB}}(m,n) = \left| 10\log_{10}\left(\frac{S_{\mathrm{yy}_{\mathrm{Optimized,Re}}}(i,p)}{S_{\mathrm{yy}_{\mathrm{Field,Re}}}(i,p)} \right) \right| + \left| 10\log_{10}\left(\frac{S_{\mathrm{yy}_{\mathrm{Optimized,Im}}}(i,p)}{S_{\mathrm{yy}_{\mathrm{Field,Im}}}(i,p)} \right) \right| \tag{1.10}$$

where $S_{\mathrm{yy}_{\mathrm{Optimized,Re}}}$ denotes the real component of the optimized output CPSD, $S_{\mathrm{yy}_{\mathrm{Optimized,Im}}}$ the imaginary component of the optimized output CPSD, $S_{\mathrm{yy}_{\mathrm{Field,Re}}}$ the real component of the field output CPSD, and $S_{\mathrm{yy}_{\mathrm{Field,Im}}}$ the imaginary component of the field output CPSD. In Eqs. (1.9) and (1.10), $\mathrm{Error}_{\mathrm{dB}}$ denotes a matrix containing the dB error for each element of $S_{\mathrm{yy}_{\mathrm{Optimized}}}$, $\mathrm{Error}_{\mathrm{dB,\,UT}}$ is the upper triangular terms of $\mathrm{Error}_{\mathrm{dB}}$ to prevent cross-terms from being counted twice, and W is a weighting matrix to apply the cross-term weighting designated for the optimization process. i and p signify the row and column index of an element of the matrices in Eq. (1.10), respectively. The output CPSD mean squared error (MSE) objective function is defined as:

$$\mathrm{OF}_{\mathrm{MSE}} = \frac{\mathrm{sum}\left(\left\| S_{\mathrm{yy}_{\mathrm{Optimized}}} - S_{\mathrm{yy}_{\mathrm{Field}}} \right\|^2 \right)}{\mathrm{numel}\left(\mathrm{S}_{\mathrm{yy}_{\mathrm{Optimized}}} \right)} \tag{1.11}$$

and the output APSD sum error objective function is

$$\mathrm{OF}_{\mathrm{Sum}} = \left\| \mathrm{sum}\left(G_{\mathrm{yy}_{\mathrm{Optimized}}} \right) - \mathrm{sum}\left(G_{\mathrm{yy}_{\mathrm{Field}}} \right) \right\| \tag{1.12}$$

where $G_{\mathrm{yy}_{\mathrm{Optimized}}}$ denotes the optimized output APSD and $G_{\mathrm{yy}_{\mathrm{Field}}}$ the field output APSD.

Figure 1.3 provides the objective function surfaces for the objective functions presented in Eqs. (1.9), (1.10), (1.11), and (1.12) at the 400 Hz frequency line and a cross-term weight of 0.25 used for the dB error calculations. Using dB error creates a surface with a larger range of values and maximum gradients, by a factor of at least 300%, at the frequency line shown. Qualitatively, the surface is more complex with a smaller number of points close to the minimum objective function, improving the resulting APSD sum calculation as well as the noise observed in the output CPSD from the determined input, which is discussed further in Sect. 1.5. For the two input locations considered, $L_{\mathrm{vec,\,dv}}$ contains a three-term vector

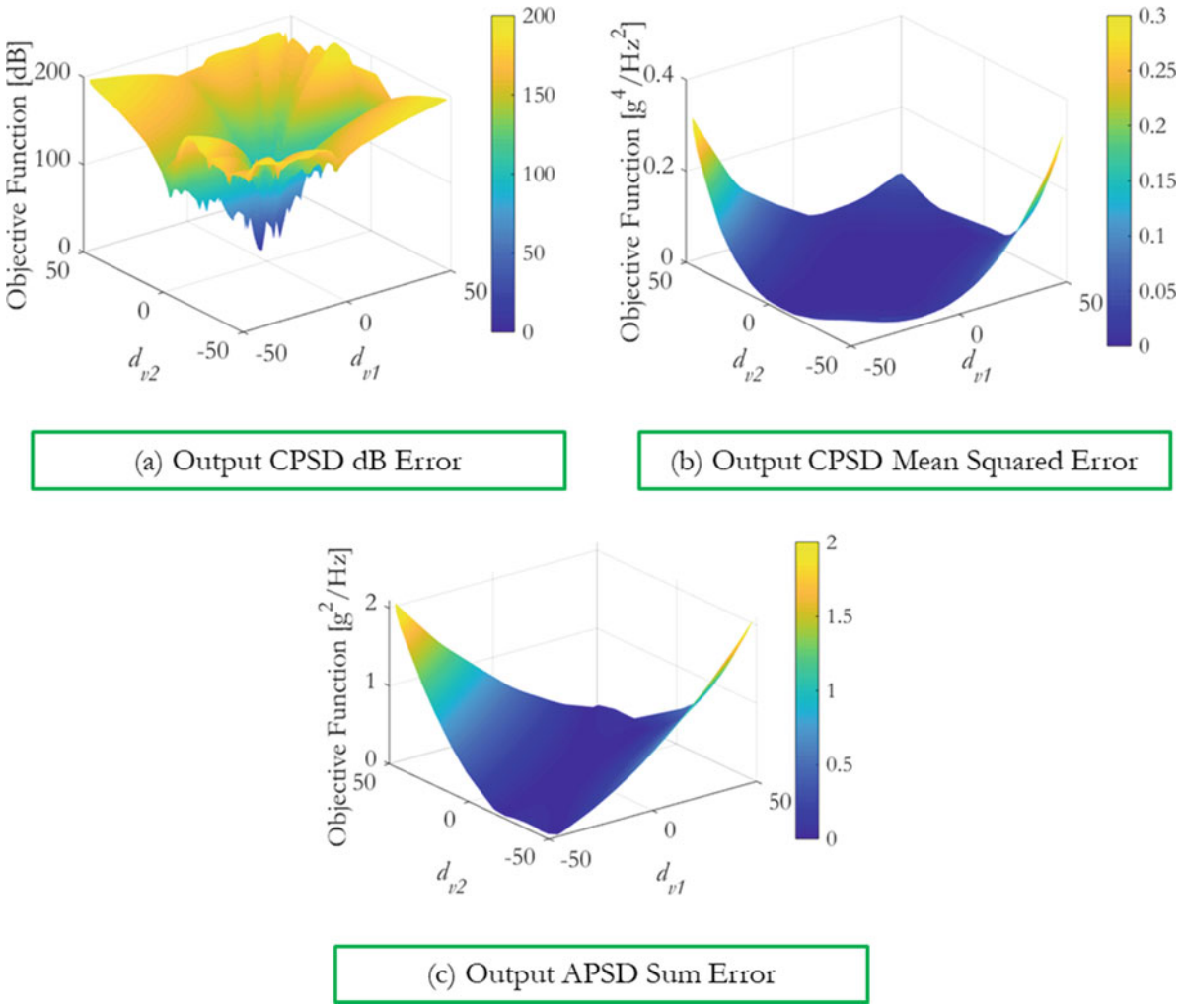

Fig. 1.3 Objective function surfaces created with LHS for objective functions based on (**a**) output CPSD dB error, (**b**) output CPSD mean squared error, and (**c**) output APSD sum error

representing $L_{\text{vec, Re}}$ and a single value representing $L_{\text{vec, Im}}$. The surfaces shown in this section vary the first two terms of $L_{\text{vec, dv}}$.

The dB error objective function maintains similar shapes as the frequency is varied through the required range. Fig. 1.4 compares the dB error objective function surface created when sampling over two of the four components of $L_{\text{vec, dv}}$. The range of values for the objective function varies by less than 10%, and the maximum gradients remain on the same order of magnitude on both frequency lines, 150 Hz in Fig. 1.4a and 400 Hz in Fig. 1.4b.

The impact of the cross-term weight on the surface created by sampling the dB error objective function with LHS is shown in Fig. 1.5. As the cross-term weight is decreased, the range of objective function values decreases by 95%, while the maximum gradients observed as the first and second components of $L_{\text{vec, dv}}$ vary and remain within 25% of the values observed with a unity cross-term weight.

1.4 Applying Iterative Optimization to MIMO Control Problem

1.4.1 Impact of Optimization Algorithm on Output CPSD

DAKOTA contains various optimization algorithms that can be leveraged to solve the iterative optimization problem for a MIMO control input [6]. The DAKOTA *.inp file is used to define the solver and related parameters and to call a MATLAB

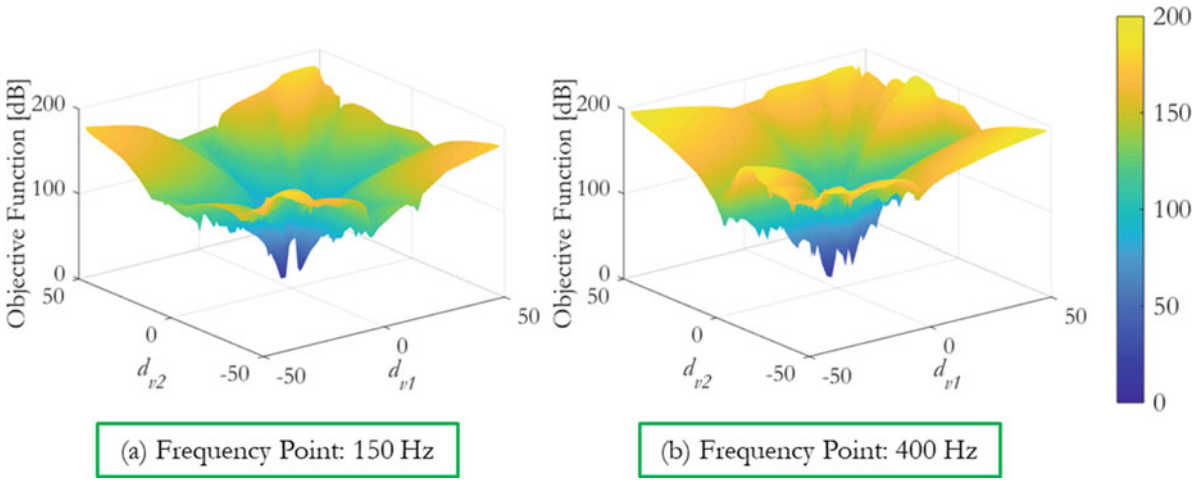

Fig. 1.4 Output CPSD dB error objective function surfaces with a fixed cross-term weight of 0.25 at frequency points (**a**) 150 Hz and (**b**) 400 Hz

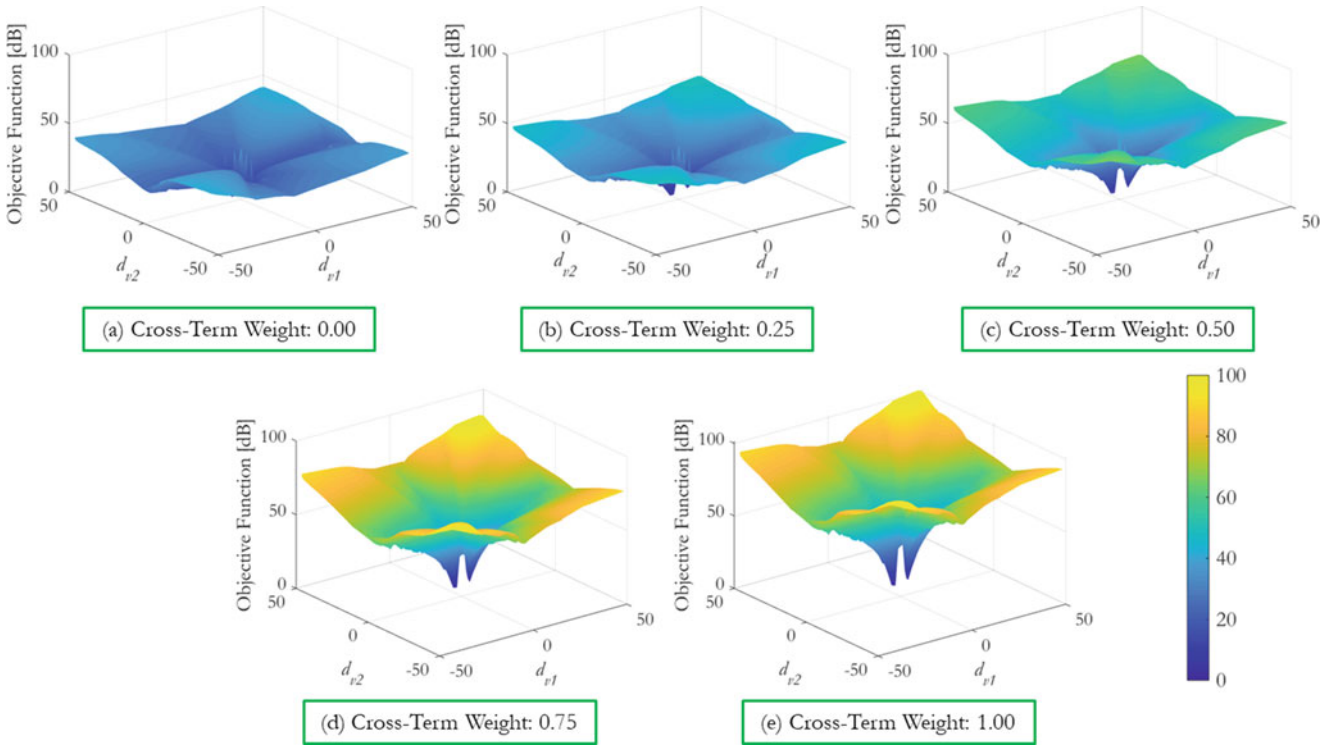

Fig. 1.5 Output CPSD dB error objective function surfaces with fixed cross-term weights of (**a**) 0.00, (**b**) 0.25, (**c**) 0.50, (**d**) 0.75, and (**e**) 1.00

wrapper that is used to complete the calculations outlined in Sect. 1.2. A simple visual basic file is used to iteratively call DAKOTA to complete the optimization process at each frequency line throughout the frequency range of interest. Solvers implemented in the example problem introduced are:

- SOGA: Single-objective genetic algorithm.
- COLINY EA: Evolutionary algorithm contained in the Sandia Colin Optimization Library (SCOLIB) collection of nongradient-based optimizers that support the Common Optimization Library Interface (COLIN).
- COLINY PS: Derivative-free pattern search included as part of SCOLIB collection of nongradient-based optimizers.
- CONMIN FRCG: Gradient-based optimization approach.

where [6] provides further details on development and implementation of these and other solvers. Table 1.1 provides a comparison at a single frequency line at 400 Hz to observe the performance of the algorithms in the high-frequency region

Table 1.1 Comparison of objective function reduction obtained with each of the solution algorithms

Algorithm	Frequency [Hz]	Cross-term weight	OF reduction [%]
SOGA	400	0.25	92%
COLINY EA	400	0.25	97%
COLINY PS	400	0.25	75%
CONMIN FRCG	400	0.25	75%

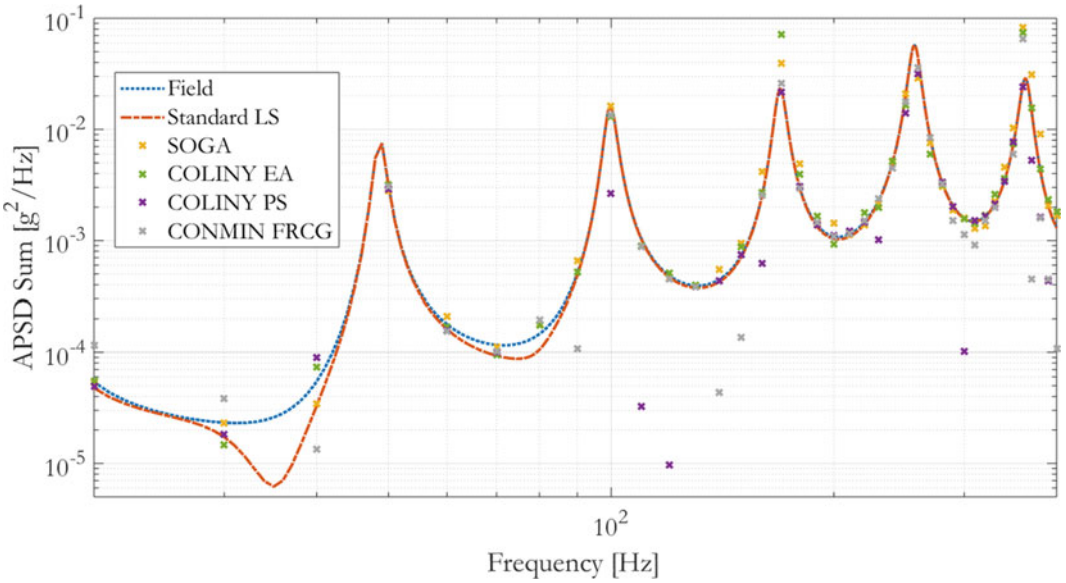

Fig. 1.6 Impact of optimization algorithm on solution obtained for MIMO control input with dB error objective function and a fixed cross-term weight

where large deviations and noise are observed. Figure 1.6 shows the impact of implementing each of these solvers on the payload example and the resulting APSD sum. The objective function used in all the cases shown in Fig. 1.6 and Table 1.1 is dB error, shown in Eqs. (1.9) and (1.10), with a fixed cross-term weight of 0.25. In the optimization runs presented in the following sections, the values of the real components of $L_{\text{vec, dv}}$ are varied from 1.0e-05 to 5, and the imaginary components are varied from −100 to 100. The initial guess for $L_{\text{vec, dv}}$ is defined so that all real components have a value of 0.05 and the imaginary component is 0. With the complex surface of the dB error objective function, the two evolutionary algorithms, SOGA and COLINY EA, outperform the gradient-based CONMIN FRCG and pattern search method, COLINY PS, with reductions of the objective function from its initial value being at least 20% more these evolutionary algorithms.

The APSD sum obtained using the evolutionary algorithms more closely follows that of the field or APSD sum obtained with standard least squares (LS), which can be observed in Fig. 1.6. Standard LS is the direct pseudoinverse method of obtaining the input CPSD. Using the COLINY EA, the solution technique improved objective function reduction in Table 1.1 and the APSD sum tracking performance presented in Fig. 1.6 by at least 5% when comparing it to the other evolutionary algorithm, SOGA. When comparing the results of COLINY EA to CONMIN FRCG, the objective function reduction is improved by more than 20%, and the average percent difference for the APSD sum calculation with the field is reduced by over 10%.

Figure 1.7 provides the objective function value obtained with the various solvers as a function of frequency. The COLINY EA solver maintains the best performance throughout the complete frequency range observed. COLINY EA results in a reduction of the mean objective function value of 63% and 29% compared to SOGA and CONMIN FRCG, respectively. Due to its increased performance, COLINY EA was chosen as the default solver to use in the development of a MIMO control input through iterative optimization. In the comparisons presented in Figs. 1.6 and 1.7, the solver options were chosen in order to result in the same order of magnitude of computation time, around 1 minute of computation time for one frequency line. In the evolutionary algorithms, COLINY EA and SOGA, the same population size and maximum function evaluation parameter were used, 100 and 2000, respectively. A 10 Hz frequency step was used in all cases.

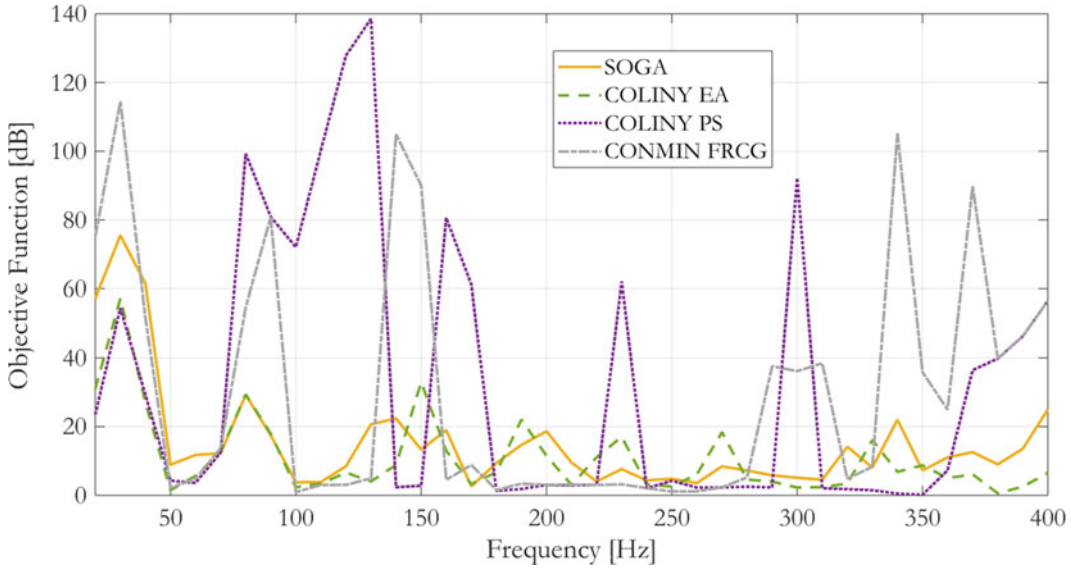

Fig. 1.7 Impact of optimization algorithm on objective function value as a function of frequency

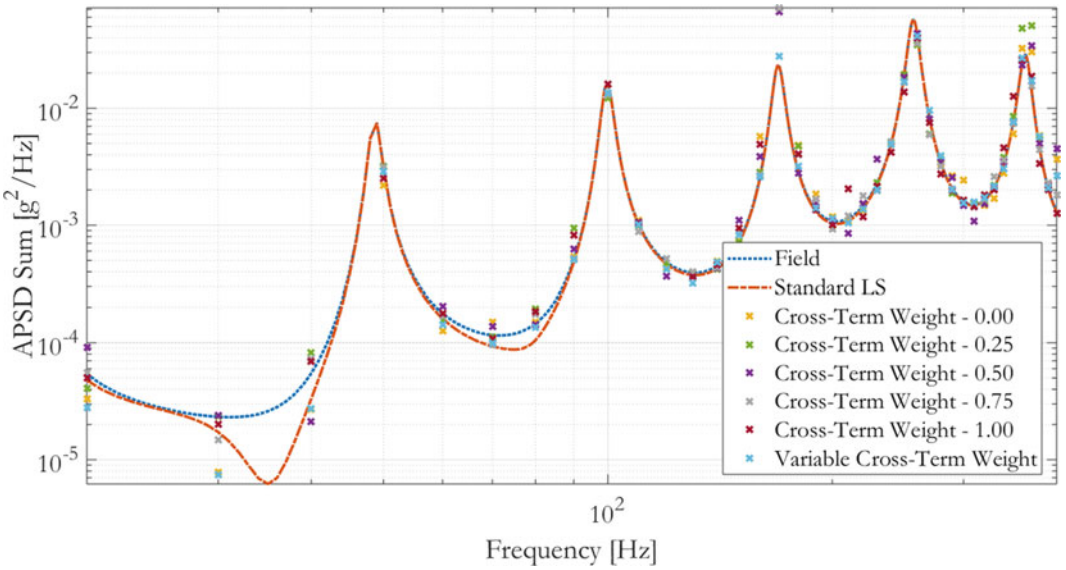

Fig. 1.8 Impact of cross-term weight on solution obtained for MIMO control input with dB error objective function

1.4.2 Impact of Iterations and Other Optimization Parameters

Another parameter that can be varied with the dB error objective function, provided in Eqs. (1.9) and (1.10), is the cross-term weight applied with matrix *W*. Figure 1.8 shows the impact of the cross-term weight definition on tracking of the field APSD sum. The cross-term weight can either be fixed at a constant value throughout frequency or used as an additional design variable in the optimization process. Maximum and minimum percent errors stay similar as the cross-term weight is varied, but the mean percent error decreases as the cross-term weight increases, a total reduction of 18% when going from a weight of 0 to 1. The best case in reducing the error in the optimized APSD sum compared to the field is to use a variable weight that can be optimized at each frequency step.

The objective function values for each cross-term weight as a function of frequency can be observed in Fig. 1.9. Values of the objective function are directly dependent on the weighting value used; therefore, the lower the cross-term weight applied, the lower the maximum and mean objective function values. As the cross-term weight is increased from 0 to 1, both the maximum and mean objective function values throughout the frequency range increase to over 350% of their original value.

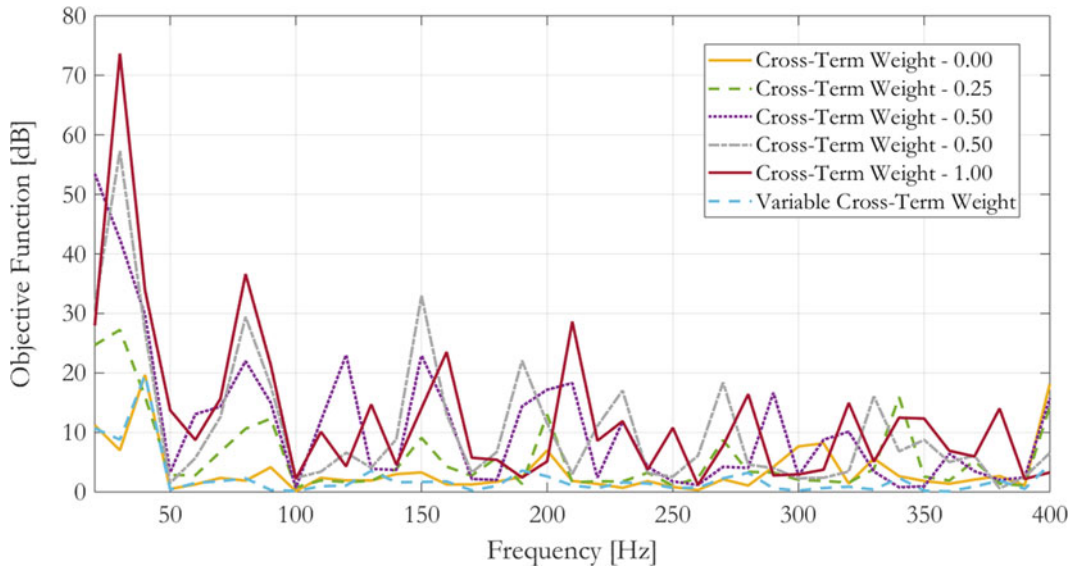

Fig. 1.9 Impact of cross-term weight on dB error objective function value as a function of frequency

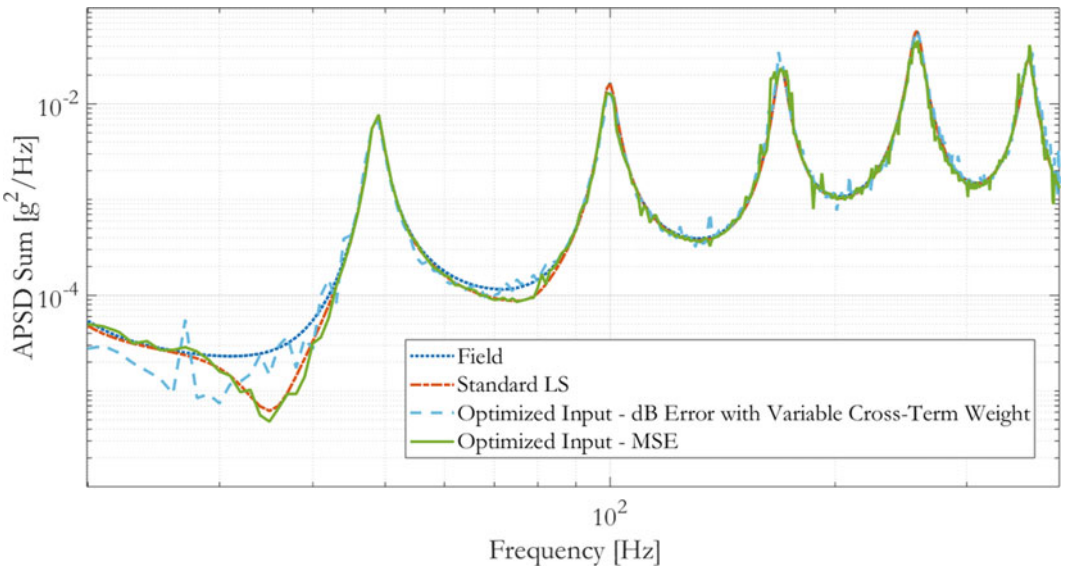

Fig. 1.10 APSD sum obtained with objective functions based on dB error with variable cross-term weights and mean squared error using a fine frequency step

Using the cross-term weight as a design variable alongside the elements of $L_{\text{vec, dv}}$ allows for the optimization process to choose the cross-term weight that allows for the lowest objective function value. Using a variable cross-term weight decreases the mean objective function value by 37% compared to a fixed cross-term weight of 0.

A fine frequency step results in smoother resulting output APSD sums, but can suffer from some slight noise based on the optimization parameters used as well as the range provided for DAKOTA to search in for each of the elements of $L_{\text{vec, dv}}$. Figure 1.10 compares the resulting APSD sum using the dB error objective function with variable cross-term weight (dashed light blue line) and the mean squared error objective function (solid green line) to the field and APSD sum acquired with the standard least squares (LS) method with a frequency step of 1 Hz. The dB error and MSE objective functions behave similar in terms of the mean percent difference between the resulting APSD sum and the field value at 13.9% and 12.7%, respectively. These values are slightly higher than the average difference of 4.29% observed when generating the MIMO control input with the standard LS method. The results of the iterative optimization, in terms of noise and error, could be improved through modification of the initial guesses at each frequency step based on previous solutions or refinement of the various optimization parameters.

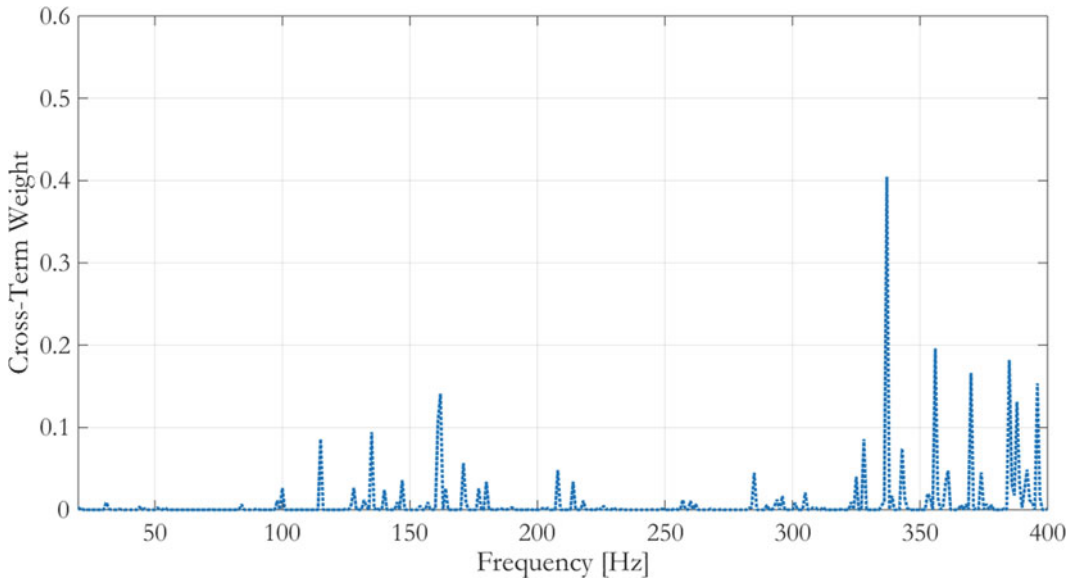

Fig. 1.11 Cross-term weight as a function of frequency chosen through optimization with DAKOTA for objective function based on dB error with variable cross-term weights

Figure 1.11 provides the resulting cross-term weight history when allowing DAKOTA and the COLINY EA solver to choose the weight at each frequency step as a design variable. In the analysis, the cross-term weight could vary from 1.00e-05 to 1, with an initial value of 0.25. The mean cross-term weight chosen in Fig. 1.11 is 0.0078 with the maximum value chosen equal to 0.4047. Above a frequency of 300 Hz, the cross-term weights tend to be larger with the maximum cross-weight occurring at 337 Hz.

1.5 Comparing Iterative Optimization to Other Methods for MIMO Control Input Development

Figure 1.12 compares the output APSD sum obtained with iterative optimization with the dB error objective function and a variable cross-term weight to several more traditional methods of generating the MIMO control input. These alternative methods include standard LS, weighted LS, and the buzz method. The buzz method is a direct pseudoinverse method where the target response CPSD cross-terms are replaced with the coherence and phase derived from the FRFs of the lab system. In terms of the mean percent difference, the best traditional method is a weighted LS method with a mean percent difference of 2.6%, which is 38.5% less than the value observed with the standard LS method. Using the dB error objective function, the mean percent difference is 13.9%. Additionally, the dB error objective function tends to follow the buzz method more closely than the other methods, especially at lower frequencies, with the mean percent difference between the optimization process and buzz method equal to 14.1%.

Figures 1.13 and 1.14 compare the traditional methods to the other objective functions presented in Sect. 1.3, mean squared error and APSD sum, respectively. Using mean squared error as an objective function results in an output APSD sum that closely follows the solution provided with standard and weighted LS. The mean percent difference between the field and the output APSD sum obtained with the mean squared error objective function is 12.7%. Comparing the result obtained with optimization and the MSE objective function to the methods based on LS, the mean percent difference is 10.1% and 11.01% for the standard and weighted LS methods, respectively. Observing Fig. 1.14, an objective function based on APSD sum error has inherently more noise compared to the other two objective functions using the same optimization parameters and design space. Additionally, the mean percent difference between the optimization methods with the output APSD sum to the field value is increased to 63.1%, which is over 45% more than the other two objective functions.

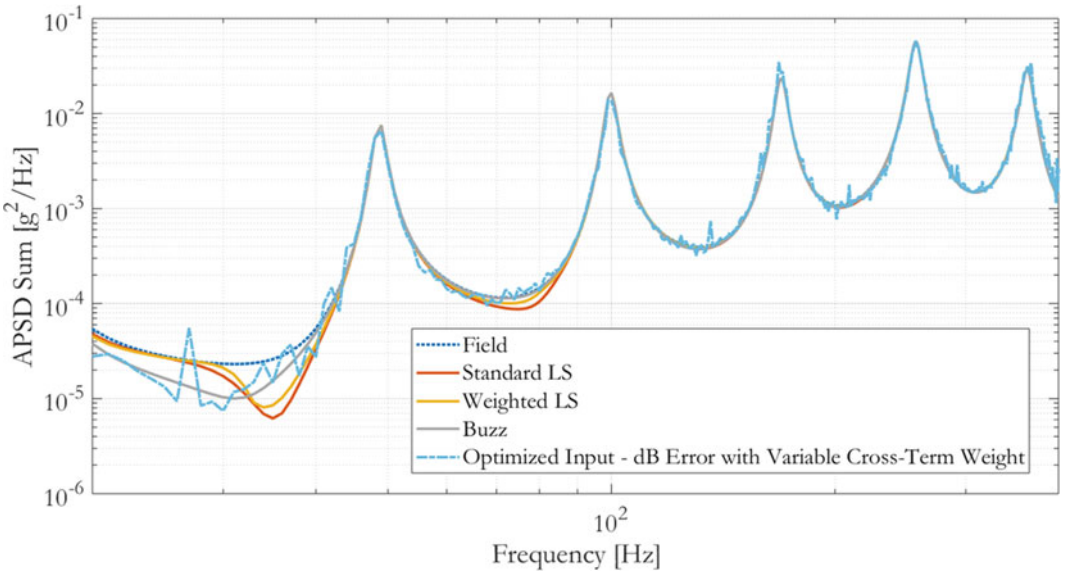

Fig. 1.12 Comparing APSD sum obtained with objective functions based on dB error with variable weight to traditional methods of obtaining MIMO control input

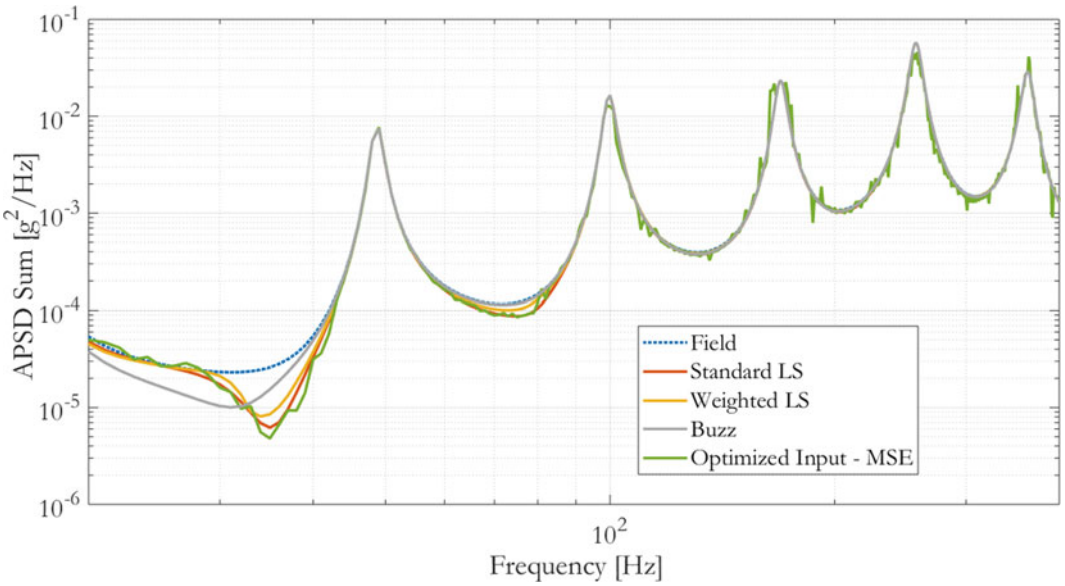

Fig. 1.13 Comparing APSD sum obtained with objective functions based on mean squared error to traditional methods of obtaining MIMO control input

Based on Figs. 1.12, 1.13, and 1.14, iterative optimization with either the dB error objective function with variable weight or MSE results in performance that is comparable to traditional, direct pseudoinverse methods. As stated previously, the error observed in the iterative optimization cases could be improved by increasing the design space of the optimization problem, improving initial guesses through previous frequency step solutions, or altering the optimization parameters. Additionally, constraints can be applied to control the input magnitude, shaker voltage, or other parameter during the optimization process, which is introduced in the following section.

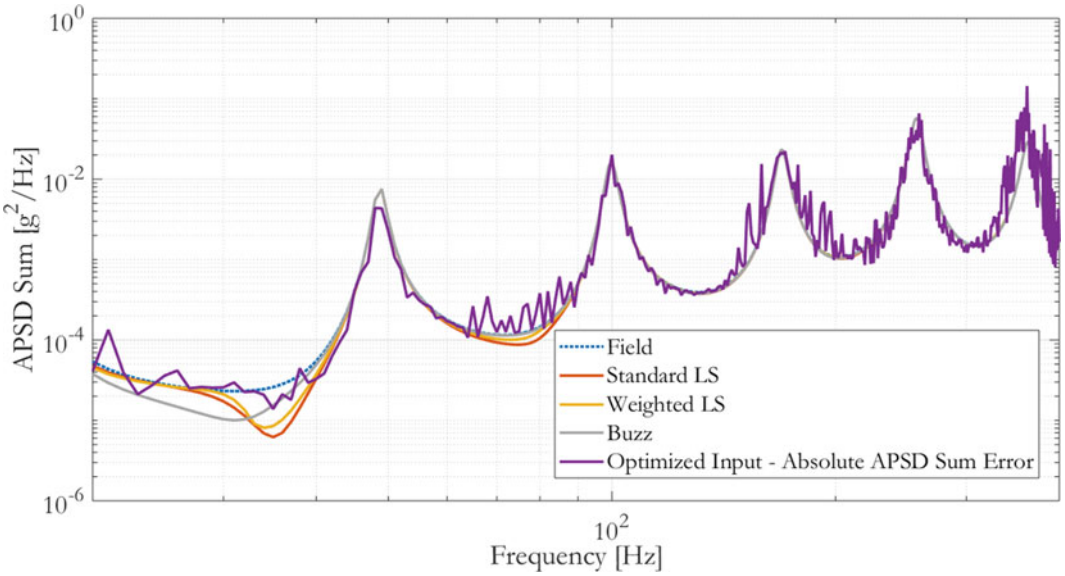

Fig. 1.14 Comparing APSD sum obtained with objective functions based on absolute APSD sum error to traditional methods of obtaining MIMO control input

1.6 Accounting for Experimental Limitations in Optimization Application

1.6.1 Directly Constraining MIMO Control Input

Constraints can be applied within the optimization process using inequality constraints. One of the most straightforward constraints to apply is the magnitude of the input CPSD, where magnitude is defined with the 2-norm. This could be done to limit the input based on the maximum force of the shaker. Figure 1.15 provides the magnitude of the input CPSD defined through optimization as a function of frequency with varying constraints. Restricting the input CPSD magnitude to 1187.2 N^2/Hz decreases the peak and mean values of the input CPSD magnitude by 65% and 24%, respectively. Further limiting the input CPSD magnitude to 494.7 N^2/Hz increases the reduction of the peak and mean values to 75.7% and 33.7%, respectively. These reductions come at the cost of increasing the objective function values obtained through optimization by 11%, which can be observed in Fig. 1.16. The impact on the mean percent difference between the output APSD sum and the field is less than 10% while maintaining the input CPSD magnitude below the specified values.

1.6.2 Accounting for Shaker Limitations with Electromechanical Model

The lumped parameter electromechanical model shown in Fig. 1.17 combines the mechanical system in Fig. 1.17a with the circuit in Fig. 1.17b and is represented using the following differential equation:

$$[M_{\text{Shaker}}]\begin{Bmatrix}\ddot{x}_1\\ \ddot{x}_2\\ \ddot{x}_3\\ \ddot{I}\end{Bmatrix}+[C_{\text{Shaker}}]\begin{Bmatrix}\dot{x}_1\\ \dot{x}_2\\ \dot{x}_3\\ \dot{I}\end{Bmatrix}+[K_{\text{Shaker}}]\begin{Bmatrix}x_1\\ x_2\\ x_3\\ I\end{Bmatrix}=\begin{Bmatrix}F_1\\ F_2\\ F_3\\ e\end{Bmatrix} \tag{1.13}$$

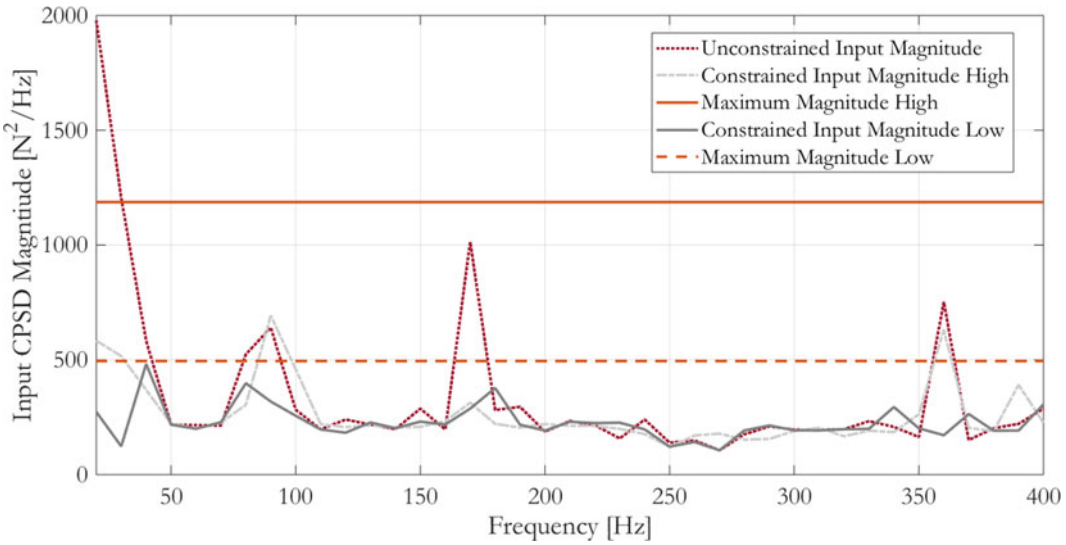

Fig. 1.15 Constrained input CPSD magnitude with various limits during optimization with objective function based on dB error with a fixed cross-term weight of 0.75

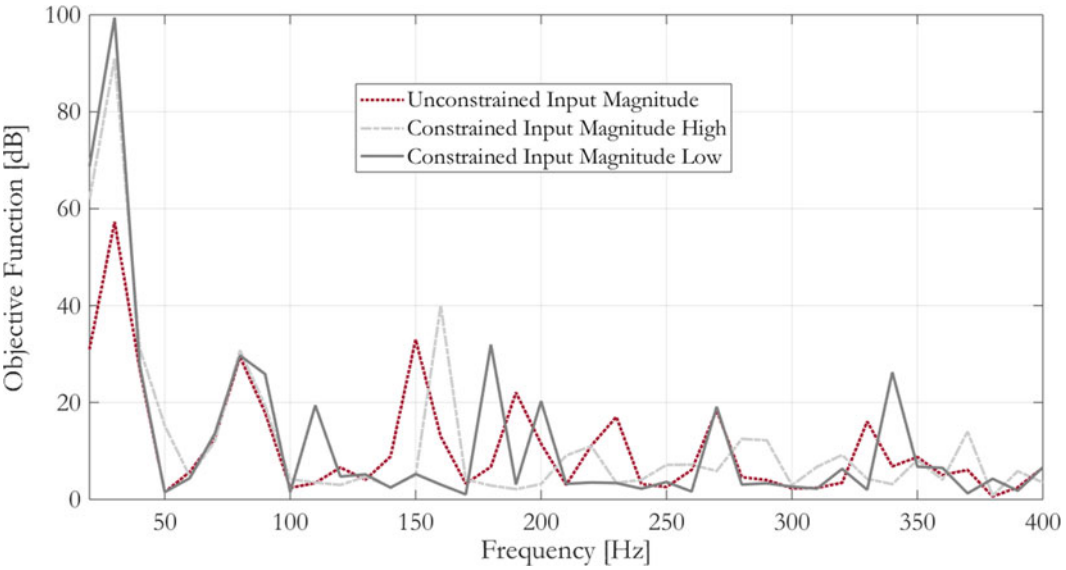

Fig. 1.16 Impact of constraining the input CPSD magnitude during optimization on objective function based on dB error with a fixed cross-term weight of 0.75

where the mass (M_{Shaker}), damping (C_{Shaker}), and stiffness (K_{Shaker}) matrices are defined as:

$$[M_{\text{Shaker}}] = \begin{bmatrix} m_1 & 0 & 0 & 0 \\ 0 & m_2 & 0 & 0 \\ 0 & 0 & m_3 & 0 \\ 0 & 0 & 0 & 0 \end{bmatrix} \tag{1.14}$$

$$[C_{\text{Shaker}}] = \begin{bmatrix} (c_{12} + c_{13}) & -c_{12} & -c_{13} & 0 \\ -c_{12} & c_{12} & 0 & 0 \\ -c_{13} & 0 & c_{13} & 0 \\ f_{\text{EMF}} & -f_{\text{EMF}} & 0 & L \end{bmatrix} \tag{1.15}$$

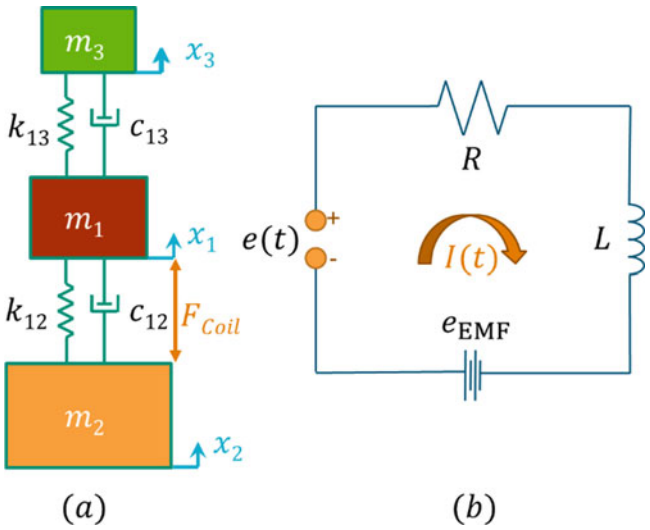

Fig. 1.17 (**a**) Mechanical components and (**b**) electrical circuit of lumped parameter electromechanical shaker model presented and calibrated in [7]

Table 1.2 Shaker parameters used in input force and voltage constraints

Parameter	Value	Units
m_1	0.44	kg
m_2	15	kg
m_3	2.6	kg
k_{12}	1.10E+04	N/m
k_{13}	6.84E+06	N/m
c_{12}	9.6	N/(m/s)
c_{13}	0.1	N/(m/s)
R	4	Ohm
L	5.00E-04 + 6.00E-04*j	Henry
f_{Force}	36	N/A

$$[K_{\text{Shaker}}] = \begin{bmatrix} (k_{12}+k_{13}) & -k_{12} & -k_{13} & -f_{\text{Force}} \\ -k_{12} & k_{12} & 0 & f_{\text{Force}} \\ -k_{13} & 0 & k_{13} & 0 \\ 0 & 0 & 0 & R \end{bmatrix} \tag{1.16}$$

In Eq. (1.13), $\dot{(\,)}$and $\ddot{(\,)}$ denote the first and second time derivatives, respectively. The connection of the electric subsystem to the mechanical subsystem is the coil force, F_{Coil}, which is defined as the product of the force factor (f_{Force}) and the current in the circuit provided in Fig. 1.17b. This connection also creates a voltage drop in the form of e_{EMF}, which is defined as $f_{\text{EMF}}(\dot{x}_1 - \dot{x}_2)$, where f_{EMF} denotes a constant accounting for the velocity dependence of e_{EMF}. The magnitude of f_{EMF} is defined to be equal to f_{Force} in the model tuning conducted in [7] with units of Vs/m. k_{12} and k_{13} are the stiffness of the springs connecting Mass 1 (m_1) to Mass 2 (m_2) and Mass 3 (m_3), respectively. c_{12} and c_{13} represent the damping between m_1 and m_2 and m_1 and m_3, respectively. L and R are the impedance and resistance in the circuit in Fig. 1.17b, respectively. x_1, x_2, and x_3 in Eq. (13) denote the displacements of Mass 1, Mass 2, and Mass 3, respectively. I and e in Eq. (1.13) are the current and voltage input in the circuit shown in Fig. 1.17b, respectively. Table 1.2 provides the parameter definitions used in Eqs. (1.13), (1.14), (1.15), and (1.16) [7, 8]. F_1, F_2, F_3 are defined to be zero since there are no external forces in this case [7].

The complete transfer function matrix resulting from the system outlined in Eqs. (1.13), (1.14), (1.15), and (1.16) is:

$$[H_{\text{Shaker}}] = \left[-\omega^2 [M_{\text{Shaker}}] + j\omega [C_{\text{Shaker}}] + [K_{\text{Shaker}}]\right]^{-1} \tag{1.17}$$

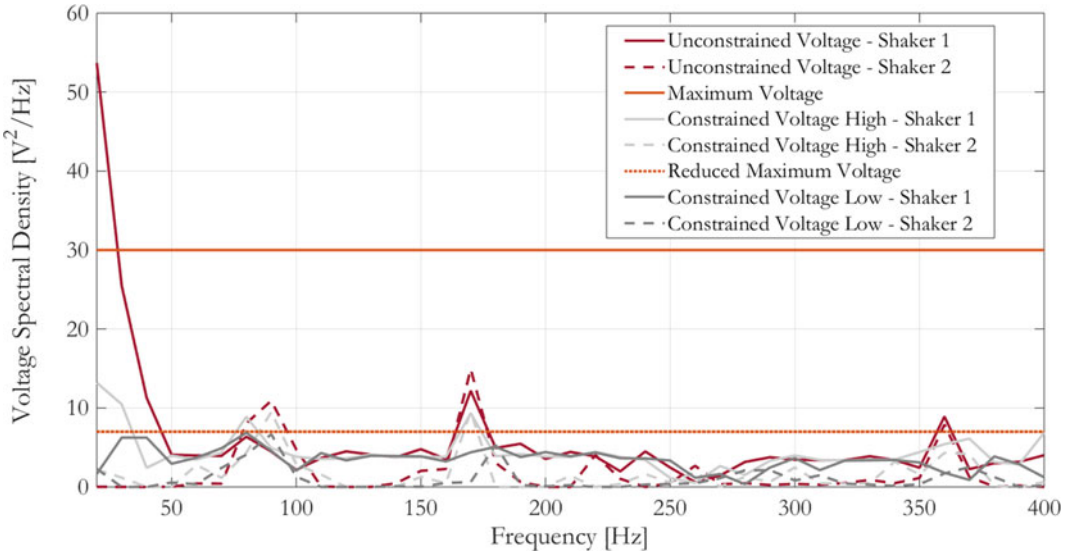

Fig. 1.18 Constrained shaker voltage with various limits during optimization with objective function based on dB error with a fixed cross-term weight of 0.75

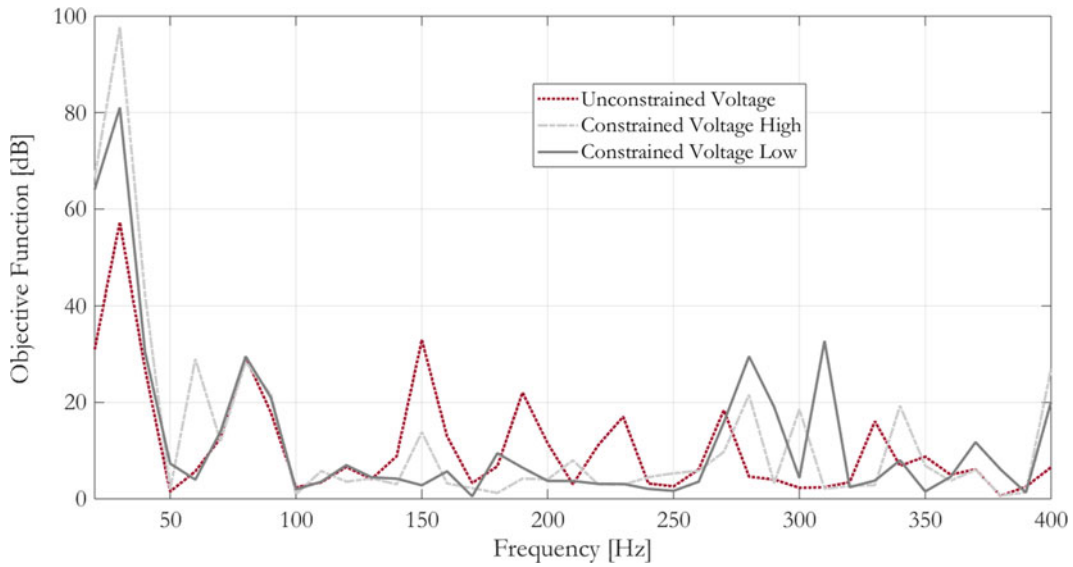

Fig. 1.19 Impact of constraining the shaker voltage during optimization on objective function based on dB error with a fixed cross-term weight of 0.75

Components of this matrix can be used to define the transfer functions needed to relate the shaker voltage and force to the input required from the shakers. The transfer function relating the voltage in the circuit shown in Fig. 1.17b to the force applied to the test article can be expressed as [7]:

$$H_{\mathrm{F_{Stinger}},\mathrm{e}} = k_{13}\left(H_{x_3,e} - H_{x_1,e}\right) \tag{1.18}$$

which can be used along with components of H_{Shaker} to approximate the shaker voltage required to impart the attached location of the test article with the correct force.

Using the transfer functions relating the stinger force of the shaker to the voltage, constraints can be defined to limit the shaker voltage in the optimization process. Figure 1.18 plots the voltage spectral density for both shakers under varying constraints with the corresponding objective function values as a function of frequency provided in Fig. 1.19. Inequality constraints limiting the voltage spectral density below 30 V^2/Hz and 7 V^2/Hz are successfully applied in Fig. 1.18. Restricting the voltage increases the mean objective function value by 12% and 17% compared to the unconstrained case for the low and

high constraints, respectively. The high constraint (30 V^2/Hz) increases the mean percent difference in the output APSD sum from the field value by 24.1%, and the low constraint (7 V^2/Hz) reduces the mean percent difference by 26.2%. Constraints on the shaker voltage can have a larger impact on the ability of the optimization process to generate effective inputs for matching field measurements compared to limits applied to the input CSPD magnitude. However, implementing these constraints in the optimization process allows for solutions to be obtained that mitigate the increase in error of the output APSDs, and in some instances can improve the results if the original solution overestimated the response. In each case, the ability of applying various shaker constraints while maintaining an effective MIMO control input provides additional flexibility to the test engineer without undue burden in the design process.

1.7 Conclusions and Future Work

Iterative optimization is an effective alternative to traditional methods in obtaining the input CPSD to best match response of a lab test article to a set of field response data. Using an objective function based on dB error or mean squared error results in mean percent errors in the APSD sum calculated with the developed input that are comparable to several traditional methods, roughly within 10% of the error seen in the traditional methods. The results obtained through the iterative optimization process are dependent on the parameters chosen for the optimization algorithm as well as the initial guess for the solution. Objective function minimization and tracking performance of the solution with the field output APSDs can be improved by increasing the initial population size alongside the allowable function evaluations as well as informing the initial guess for each frequency step based on previous solutions. Additionally, using iterative optimization to acquire the input CSPD for a field environment allows for constraints to be applied alongside the process to maintain the input CPSD magnitude or shaker voltages below a predefined level allowing for a test engineer to account for limitations in test setups and test equipment, like shakers and amplifiers. These limitations can be accounted for while maintaining efficacy by mitigating the impact to the error metric or tracking performance of the output APSDs. The additional flexibility provided by these iterative optimization techniques comes at a cost. The computation time required to determine a solution using an iterative optimization technique is much greater than the time required for direct pseudoinverse solutions. Future work can focus on improving the quality of the initial guesses at each frequency step based on previous solutions, exploring methods to decrease dependency of the method on the forward MIMO control problem, and implementing the method on complex systems with many input points.

References

1. Daborn, P.M., Ind, P.R., Ewins, D.J.: Enhanced ground-based vibration testing for aerodynamic environments. Mech. Syst. Signal Process. **49**(1–2), 165–180 (2014)
2. Whiteman, W., Berman, M.: Inadequacies in uniaxial stress screen vibration testing. J. IEST. **44**(4), 20–23 (2001)
3. Roberts, C., Ewins, D.J.: Multi-axis vibration testing of an aerodynamically excited structure. J. Vib. Control. **24**(2), 427–437 (2018)
4. Ross, M., Jacobs, L.D., Tipton, G., Nelson, G., Cross, K., Hunter, N., Harvie, J.: 6-DOF shaker test input derivation from field test. In: Shock & Vibration, Aircraft/Aerospace, Energy Harvesting, Acoustics & Optics, Volume 9, pp. 11–22. Springer, Cham (2017)
5. Daborn, P.M.: Scaling up of the impedance-matched multi-axis test (IMMAT) technique. In: Shock & Vibration, Aircraft/Aerospace, Energy Harvesting, Acoustics & Optics, Volume 9, pp. 1–10. Springer, Cham (2017)
6. Adams, B., et al.: Dakota 6.10 Reference Manual Documentation. Retrieved April 14, 2019 from https://dakota.sandia.gov/content/latest-reference-manual (2019)
7. Schultz, R.: Calibration of shaker electro-mechanical models. In: Special Topics in Structural Dynamics & Experimental Techniques, Volume 5, pp. 133–144. Springer, Cham (2019)
8. Tiwari, N., Puri, A., Saraswat, A.: Lumped parameter modeling and methodology for extraction of model parameters for an electrodynamic shaker. J. Low Freq. Noise Vib. Active Control. **36**(2), 99–115 (2017)